JCTC Journal of Chemical Theory and Computation

ARTICLE

pubs.acs.org/JCTC

Effects of Spin−Orbit Coupling on Covalent Bonding and the Jahn−Teller Effect Are Revealed with the Natural Language of Spinors

Tao Zeng,[†] Dmitri G. Fedorov,[‡] Michael W. Schmidt,[§] and Mariusz Klobukowski*[,†]

[†]Department of Chemistry, University of Alberta, Edmonton, Alberta, Canada, T6G 2G2

[‡]NRI, National Institute of Advanced Industrial Science and Technology (AIST), Central 2, Umezono 1-1-1, Tsukuba, 305-8568, Japan

[§]Department of Chemistry and Ames Laboratory USDOE, Iowa State University, Ames, Iowa 50011, United States

ABSTRACT: The orbital-based natural language describing the complexity of chemistry (Stowasser, R.; Hoffmann, R. *J. Am. Chem. Soc.* **1999**, *121*, 3414) was extended by us recently to the definition of spin−orbit natural spinors (Zeng, T. et al. *J. Chem. Phys.* **2011**, *134*, 214107). This novel method gives chemical insights into the role of spin−orbit coupling in covalent bonding and in the Jahn−Teller effect. The natural spinors are used to explain antibonding spin−orbit effects on TlH and Tl_2: it is found that the spin−orbit induced charge transfer from the bonding to the nonbonding or antibonding orbitals has a large effect on the bond strength. The natural spinors are also used to explain the spin−orbit quenching of the Jahn−Teller effect in WF_5: the spin−orbit interaction can stabilize the totally symmetric electron distribution so that the high-symmetry molecular structure becomes more stable than its distortions. A general discussion of the role of the spin−orbit coupling in covalent bonding and Jahn−Teller effect is given in terms of the competition between the rotational nature of the spin−orbit coupling and the directionality of the two effects. The natural spinors offer the advantage of providing a simple and clear pictorial explanation for the profound relativistic spin-dependent interactions in chemistry often appearing as a black box answer.

1. INTRODUCTION

The special theory of relativity leads to very profound effects in chemistry.[1−4] The relativistic effects can be divided into two categories: the scalar-relativistic and the spin-relativistic effects. The manifestations of the former effect are, for example, the liquid state of mercury under ambient temperature and pressure,[5] the golden color of gold,[6−8] and the inertness of the $6s^2$ electron pair.[9] Since the operators describing the scalar-relativistic effects do not introduce new symmetry, they are relatively easy to implement in the conventional quantum chemistry programs, and their interpretation is facilitated by that. The spin-relativistic effect, however, introduces the double group symmetry[10,11] related to the electron spin of 1/2, forms one of the obstacles in current development of quantum chemistry, and presents difficulties in the conceptual interpretation of the "black box" results. The importance of a tool giving a simple representation of a complex phenomenon cannot be overestimated; a chemist wants to understand not only what happens but also why and be able to form a mental picture of the complex chemical processes caused by complicated physical concepts. Among the spin-related operators, the spin−orbit coupling typically has the largest magnitude.[12] The circulation of an electron around a nucleus in the reference frame of the electron can be considered a circulating motion of the nucleus around the electron, which creates a magnetic field. On the other hand, the electronic spin creates a magnetic dipole moment. The coupling between the magnetic field and the magnetic dipole moment leads to the spin−orbit coupling (see section 1.3.3 of ref 13 for a detailed discussion). The spin−orbit coupling manifests itself in several phenomena in chemistry:[12,14] the fine structure splitting, intersystem crossing, and spin-forbidden radiative transition. Because this interaction increases with the nuclear charge,[15,16] a proper study of the heavy element chemistry often requires taking this interaction into account.

There are two strategies for spin−orbit coupling calculations: the so-called one-step[17−19] and two-step methods.[20−25] The advantage of the one-step coupling scheme is that the spin−orbit effects are included in the orbital optimization yielding $j-j$ spinors. The influence of this interaction on the wave function can be directly analyzed, which is important as the orbitals provide a *natural language*[26] for the complexity of chemistry. In contrast, the two-step coupling first generates a set of states (Russell−Saunders terms) with a definite total spin quantum number S for the spin part and a point group symmetry label Γ for the spatial part of the wave function. Subsequently, the spin−orbit coupling effect is added at a post-Hartree−Fock level taking the Russell−Saunders terms (Γ-S states) as the multielectron basis functions.[16,27] In this way, the two-step coupling scheme can be easily implemented in typical nonrelativistic quantum-chemical programs, so their impressive development of the electron correlation methodology can be easily incorporated into spin−orbit calculations. However, the action of the spin−orbit operator on the wave function is represented by the mixing of the Russell−Saunders terms, and the orbital-based analysis cannot be applied. Recently, we developed an algorithm[28] to calculate the natural orbitals for two-step coupled wave functions, and these natural spinors have been shown to closely mimic the corresponding $j-j$ spinors. This new technique allows one to obtain a $j-j$ spinor analogue in a two-step coupled wave function, and the advantages of both coupling schemes are then combined.

Following our recent derivation and algorithm of the natural spinor methodology, we present here the first chemical applications of this new technique. There are two interesting problems related to spin−orbit interaction that have fascinated chemists

Received: June 30, 2011
Published: August 05, 2011

for a long time: the interplay between the spin−orbit and the bonding interactions[29−39] and the interplay between the spin−orbit and the Jahn−Teller effect.[40−51] Spin−orbit interaction often lifts the electronic degeneracy and transforms the Jahn−Teller effect into a pseudo-Jahn−Teller effect. In the present work, we apply the natural spinors to illuminate the details of these two phenomena. As shown below, the natural spinors capture the role of spin−orbit coupling both in the covalent bonding and in the Jahn−Teller effect and provide deep chemical insights. Although discussions in this work are based mainly on case studies, the approach based on natural spinor analysis is general and can be applied to other systems. To be more specific, the term "bonding" only means covalent bonding interaction in this work.

This paper is arranged as follows. In section 2, we present a short review of the natural spinors and some computational details in this work. In section 3, we use the natural spinors to explain the spin−orbit antibonding effect, taking TlH and Tl_2 as examples. In section 4, we use the natural spinors to explain the spin−orbit quenching of the Jahn−Teller distortion, taking WF_5 as an example. Section 5 summarizes this work. Unless further specified, all units used in this paper are atomic units (a.u.) and "term" and "level" are used to denote the multielectron states without and with the spin−orbit interaction being considered, respectively.

2. METHODOLOGY

The concept of natural orbitals dates back well into the past.[52−54] In our recent application[28] of this concept to a two-step spin−orbit coupled wave function, the natural spinors are obtained as the eigenfunctions of the two-step spin−orbit coupled density operator. The two-step coupled wave functions are generally complex-valued and mix different spin multiplicities. As a reflection of this nature, the natural spinors are also generally complex-valued and mix the two spin components (α and β) of an electron. If all of the components of a multidimensional irreducible representation of the associated double group are equally averaged to produce the one-electron reduced density, the associated density operator is of the totally symmetric irreducible representation and commutes with all of the symmetry operators.[28,54] Consequently, its eigenvectors (natural spinors) must belong to the irreducible representations of the same double group, i.e., they must have the same symmetry properties as the $j-j$ spinors. Since the natural spinors contain the information of the two-step coupled wave function and are symmetry adapted, they are perfect candidates for wave function analysis. The details of the algorithm and test cases of the natural spinors are given in the previous publication.[28]

For general polyatomic molecules, the one-electron effective spin−orbit operator is[12]

$$\sum_{iA} \hat{V}_{iA}\, \hat{\vec{l}}_{iA} \cdot \hat{\vec{s}}_i \qquad (1)$$

where i labels the electrons, A labels the nuclei, $\hat{V}_{iA}$ stands for the coupling strength and is a function of the distance r_{iA} between electron i and nucleus A in the spatial representation, $\hat{\vec{l}}_{iA}$ is the orbital angular momentum operator of electron i around nucleus A, and $\hat{\vec{s}}_i$ is the electron spin operator. Since the two-electron spin−orbit interaction does not change the symmetry properties of the one-electron analogue,[13] eq 1 can be taken to represent both one- and two-electron operators for the symmetry analysis, with the two-electron shielding effect stored in the effective coupling strength V_{iA}. The operator $\hat{\vec{l}}_{iA}$ determines that the spin−orbit interaction exerts its effect (either lowering or raising the energy) by the electron rotation around each nucleus, since the angular momentum operator is the generator for rotation.[55]

An important concept in the present work is the spin−orbit induced electron transfer between molecular orbitals. This terminology stems from the interpretation of the matrix element $\langle \mu\lambda|\hat{V}_{iA}\, \hat{\vec{l}}_{iA} \cdot \hat{\vec{s}}_i|\nu\sigma\rangle$, where μ and ν are the spatial molecular orbitals and λ and σ are the spin components (α or β). Such matrix elements are responsible for the spin−orbit splitting in the two-step coupling scheme,[56] and they can be written as $\langle \mu|\hat{V}_{iA}\, \hat{\vec{l}}_{iA}|\nu\rangle \cdot \langle \lambda|\hat{\vec{s}}_i|\sigma\rangle$. The spin part (the matrix element after the dot) determines the spin magnetic dipole, and the spatial part (the matrix element before the dot) determines the effective magnetic field, which stems from the relative nucleus A rotation around electron i. In the space-fixed (nuclei-fixed) frame, such a relative rotation appears as the electron i rotation around nucleus A, and this explains the appearance of $\hat{\vec{l}}_{iA}$, not $\hat{\vec{l}}_{Ai}$, in eq 1. Here, we would like to emphasize that $\hat{\vec{l}}_{iA}$ is the angular momentum operator of electron i around nucleus A while $\hat{\vec{l}}_{Ai}$ is the analogue for the motion of nucleus A around electron i. For the real orbitals usually used in chemistry, only the off-diagonal matrix elements of $\langle \mu|V_{iA}\, \hat{\vec{l}}_{iA}|\nu\rangle$ are nonzero,[56,57] which means that the spin−orbit effect cannot be realized by keeping the electron in the same spatial orbital; i.e., it has to come as an electron transition between spatial orbitals.

Next, it is well-known that, in the two-step methods,[56,57] doubly occupied orbitals alone do not contribute to spin−orbit coupling, and nonzero spin−orbit matrix elements must couple Slater determinants with occupancy discoincidence of one or two orbitals, i.e., transferring electrons from occupied to virtual orbitals. This charge transfer is a manifestation of the direction change of the electron spatial distribution around a nucleus induced by the electron rotation in the spin−orbit effect. A similar notation was employed by Turro et al.[31] to visualize the action of spin−orbit coupling. We also note that, for atoms, the charge transfer can be visualized by rotations more directly, as the atomic orbitals have well-defined rotational properties suitable for this interpretation, while in molecules, the anisotropic nature of the Coulomb interaction leads to molecular orbitals with various distributions which obstruct the orbital rotation interpretation. Therefore, we refer to the action of spin−orbit coupling as electron (or charge) transfer.

Let us consider a charge (electron) transfer from an occupied orbital $\mu\sigma$ to a virtual orbital $\nu\lambda$ induced by spin−orbit coupling. By employing the second order perturbation theory formulas, the magnitude (not considering the sign) of the spin−orbit energy and wave function contributions from a transfer between a pair of orbitals can be expressed, respectively, as

$$\frac{\left|\left\langle \mu\lambda|\hat{V}_{iA}\, \hat{\vec{l}}_{iA} \cdot \hat{\vec{s}}_i|\nu\sigma\right\rangle\right|^2}{|E^0_{\nu\sigma} - E^0_{\mu\lambda}|} \text{ and } \frac{\left|\left\langle \mu\lambda|\hat{V}_{iA}\, \hat{\vec{l}}_{iA} \cdot \hat{\vec{s}}_i|\nu\sigma\right\rangle\right|}{|E^0_{\nu\sigma} - E^0_{\mu\lambda}|} \qquad (2)$$

where the denominator is the energy gap between the states in which $\mu\lambda$ or $\nu\sigma$ is occupied. This energy gap can then be approximated as the orbital energy difference between $\mu\lambda$ and

$\nu\sigma$, which leads to the explanation that the larger the energy gap between the two orbitals, the less significant the spin−orbit induced electron transfer between them.

At this point, it is necessary to compare our natural spinors and the canonical $j-j$ spinors in the one-step spin−orbit coupled calculation. The canonical spinors are obtained by diagonalizing the two-component Fock operator that has included the spin−orbit effect, and therefore, they have the associated spinor energies[17] (analogues of orbital energies in calculations without spin−orbit), which are the eigenvalues of the Fock operator. However, those canonical $j-j$ spinors in the active space have unknown occupation numbers. In contrast, our natural spinors diagonalize the density matrix of a spin−orbit wave function and have a definite occupation number for each spinor but do not have the associated orbital energy. Therefore, the natural spinors and the $j-j$ canonical spinors provide complementary information about a spin−orbit coupled wave function.

We implemented the natural spinor algorithm into GAMESS-US[58,59] and employed this open-source quantum chemistry program package to perform all of the electronic structure calculations in this work. The basis sets and the relativistic treatment are described below. The electron correlation is treated at the complete active space configuration interaction (CASCI) levels, and the corresponding SO-CASCI treatment[50] is employed to account for the spin−orbit interaction. The natural spinors are obtained from the SO-CASCI wave functions.

All orbital pictures in this work are prepared using graphical program MacMolPlt.[60] We developed a program that can create MacMolPlt data files for the complex natural spinors by dividing each of the complex spinors into four real-valued "orbitals", and the spinor's occupation number is assigned to each of the pseudo-orbitals. This program is employed to make images of the electron density for natural spinors. The four pseudo-orbitals correspond to the four phases of a spinor: real-valued function with α spin, real-valued function with β spin, imaginary-valued function with α spin, and imaginary-valued function with β spin. For example, the $p_{1/2,-1/2}$ spinor (we use the notation $l_{j,jz}$, see Table S.II in the Supporting Information of ref 28 for the definition of these prototypical atomic spinors):

$$p_{1/2,-1/2} = \sqrt{\frac{1}{3}}p_x\alpha - i\sqrt{\frac{1}{3}}p_y\alpha + \sqrt{\frac{1}{3}}p_z\beta \qquad (3)$$

requires three "orbitals" to visualize: a real α "orbital" for $(1/3)^{1/2}p_x\alpha$, an imaginary α "orbital" for $-i(1/3)^{1/2}p_y\alpha$, and a real β "orbital" for $(1/3)^{1/2}p_z\beta$. Each of the pseudo-orbitals are unnormalized, and if this $p_{1/2,-1/2}$ spinor is occupied by x ($x \leq 1$) electrons, x is assigned to the three pseudo-orbitals. One should notice that the natural spinors in this work may not have the same mathematical expression as used elsewhere, because they follow the phase convention and coordinate system of the program we use, which may not be identical to those in other programs. In the discussions below, the term "natural orbital" is reserved for the eigenvectors that diagonalize the one-electron density matrix of a non-spin−orbit wave function, while "natural spinor" is used for the spin−orbit analogues. One should be aware of the difference between the two terms.

3. HOW SPIN−ORBIT COUPLING CHANGES THE COVALENT BOND STRENGTH IN DIATOMIC MOLECULES

According to Ruedenberg et al.,[61,62,64,65] a covalent bond is formed in two steps. First, the electron sharing between atoms leads to an attenuation of the kinetic energy pressure and the associated lower ratio between kinetic and potential energies ($T/|V|$). Second, the nonequilibrium $T/|V|$ ratio leads to a wave function relaxation together with an increase of the kinetic and a decrease of the potential energy until the equilibrium $T/|V|$ ratio is attained (1/2 for the pure Coulomb interaction according to the virial theorem). The kinetic pressure attenuation when the bonded atoms approach is the ultimate reason for the covalent bonding, and an orbital deformation (polarization and contraction) and the electron correlation are important in the subsequent step. The electron occupation in a bonding orbital (with no node along the bonding direction) is the signature for kinetic pressure attenuation in the bonding region and the formation of a covalent bond.

It is known that the spin−orbit effect can alter the bond strength of molecules (see section 22.3 of ref 66 and the references therein). Two typical examples are TlH[38] and Tl_2[67] molecules, whose bond energies are greatly weakened when the spin−orbit effect is included. Conceptually, one may explain this phenomenon by the fact that the spin−orbit effect lowers the energy of the Tl $6p_{1/2}$ orbital and thus stabilizes the Tl atom at the dissociation limit. In this section, we explain this antibonding spin−orbit effect in terms of the population analysis using the natural spinors. To this end, we perform the two-step spin−orbit coupling calculations for the two molecules with the active space of the valence spin-free one-component natural orbitals and investigate the change of their electron occupation numbers. This change of occupation numbers reflects the change of the bond strength. Before going into the details, we need to emphasize that we focus on the qualitative wave function analysis by studying the natural spinors, as accurate quantitative energetics are not pursued here.

We employ a very simple model for the TlH calculation, and since this is a qualitative study, the simple model can tell us what we need to know without the entanglement of other nondetermining factors. In this model, we completely contract the well-tempered basis functions (WTBS)[68] using the atomic orbital coefficients (calculated at the relativistic level of the third order of Douglas−Kroll−Hess (DKH3) Hamiltonian[69,70]) to make the basis set for Tl and completely contract the s primitives of the aug-cc-pV5Z basis set[71] to make the basis set for H. No additional diffuse or polarization functions are added. The construction of these basis sets is similar to that of the MINI basis set,[72] providing no polarization and only near-degeneracy (often called strong) correlation within the valence orbital space, for a simple qualitative analysis illustrating the concepts. We note here that our analysis is based on occupation numbers of natural orbitals (NOs), and *the NO occupation numbers are stable quantities that do not vary much when a wave function is improved, once a wave function has been defined that includes the most important NOs.*[73] We do not involve any dynamic electron correlation in this model since correlation does not dominate in a conventional covalent bond.[62] Neglecting this effect helps to disentangle this complex interaction from the rest and focus on the interplay between spin−orbit and covalent interactions.

Using these basis sets and the active space of two electrons in the σ, σ^*, and π orbitals, we perform a complete active space self-consistent field (CASSCF) geometry optimization to find the equilibrium internuclear distance of 2.062 Å. This rather long bond length as compared to the experimental value of 1.872 Å[63] is as expected because of the unpolarized basis set used and the missing dynamic correlation. For this structure, CASCI is performed to obtain one-component natural orbitals of the ground state $^1\Sigma^+$ term, and those orbitals are depicted in Figure 1a−c with their

occupation numbers listed in Table 1. Obviously, the π orbitals are the nonbonding $6p_{x,y}$ orbitals of Tl, and the asterisk of the σ^* orbital denotes its antibonding charater. Subsequently, all Γ-S terms generated by the CASCI distributing two electrons in the four natural orbitals are included in the spin−orbit CI calculation to produce the ground state spin−orbit wave function, the 0^+ level.

Employing this active space, the 0^+ level's natural spinors can be represented by the one-component natural orbitals of the $^1\Sigma^+$ term, and their expressions and occupation numbers are:

$$\frac{1}{2} = 0.993885\sigma\alpha - 0.001369\sigma^*\alpha - 0.078072(\pi_x\beta + i\pi_y\beta), \text{occup} : 0.9641 \quad (4)$$

$$\frac{1'}{2} = -0.022310\sigma\alpha + 0.976810\sigma^*\alpha - 0.150574(\pi_x\beta + i\pi_y\beta), \text{occup} : 0.0355 \quad (5)$$

$$\frac{3}{2} = \sqrt{\frac{1}{2}}\pi_x\alpha + i\sqrt{\frac{1}{2}}\pi_y\alpha, \text{occup} : 0.0002 \quad (6)$$

$$\frac{1''}{2} = 0.108142\sigma\alpha + 0.214105\sigma^*\alpha + 0.686464(\pi_x\beta + i\pi_y\beta), \text{occup} : 0.0002. \quad (7)$$

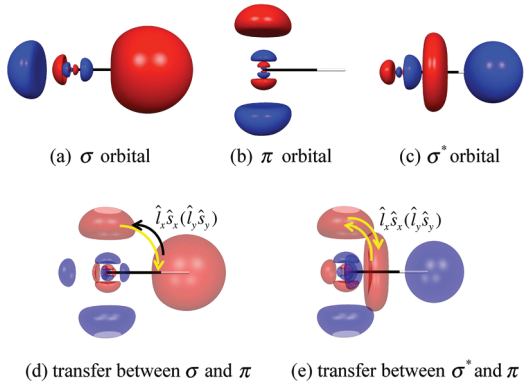

Figure 1. One-component natural orbitals from CASCI without spin−orbit coupling (a−c) for TlH, as well as the spin−orbit coupling induced electron transfer (d,e) among them. The Tl atom is on the left (black), and hydrogen on the right (white). The $\hat{l}_x$ and $\hat{l}_y$ operators are centered on the Tl atom. In d and e, if the shown π orbital is the π_y component, then the $\hat{l}_x\hat{s}_x$ operator applies and similarly for π_x and $\hat{l}_y\hat{s}_y$. Substantial electron transfers (typically, from occupied to unoccupied orbitals) are denoted by a black arrow, while the negligible ones are denoted by yellow ones.

Here, we use the ω value (the eigenvalue of the $\hat{j}_z$ operator on the left-hand side of the expressions above) to label the natural spinors and prime and double prime to differentiate the orbitals with the same ω. Since the Kramers pairs[74] (with negative ω) of the listed natural spinors have the same eigenvalues, they are omitted here, and one can apply the time-reversal operator on the listed spinors to generate them.[66,75] The effect of the time-reversal operator is to change α to β and β to $-\alpha$ and take the complex conjugate for its operand. Despite its simplicity, this model includes the primary covalent and spin−orbit interactions and serves as a good model to study the interplay between these two interactions.

To compare the one-component natural orbitals (σ, σ^*, and π) to the natural spinors of the spin−orbit 0^+ wave function, we can calculate the averaged occupation numbers (diagonal density matrix elements) for each of the natural spinors according to

$$\text{occ}_i = \sum_j \text{occ}_j |C_{ij}|^2 \quad (8)$$

where i labels the one-component natural orbitals, j labels the natural spinors, C_{ij} are the coefficients in eqs 4−7, and the summation runs over all of the natural spinors. The calculated average occupation numbers are listed in Table 1. The comparison of the occupation numbers for the $^1\Sigma^+$ and 0^+ wave functions indicates that the spin−orbit interaction causes a substantial electron transfer (0.0285) from the bonding σ orbital to the nonbonding π and antibonding σ^* orbitals. This electron transfer weakens the bond, and if we use the effective bond order model,[73,76] in which the bond order equals one-half of the total occupation number of bonding orbitals less the total occupation number of antibonding orbitals, then the TlH bond order is lowered from 0.9336 to 0.9184. Most of the depleted electron from the σ orbital (0.0270) is deposited in the nonbonding π orbitals, and this can be explained considering the detailed spin−orbit interaction. For the TlH molecule, the spin−orbit effect at the Tl nucleus is overwhelming and, focusing on the interaction around this nucleus, we label the orbital angular momentum operators centered on Tl as $\hat{\vec{l}}$. In the ground state, the spin−orbit effect must lower the energy,[12] and this stabilization is the driving force for the electron transfer.

The relevant spin−orbit induced electron transfer is illustrated in Figure 1d. Since only the σ orbital is substantially occupied in the original $^1\Sigma^+$ wave function, the net result observed is electron transfer from σ to π orbitals. Likewise, any charge originally occupying the π orbitals can be transferred to the σ^* orbital and vice versa, as illustrated in Figure 1e. Because of the insignificant occupations of the σ^* and π orbitals, the transfer between them is negligible. As $\hat{l}_z$ can only couple the two π orbitals and the electron transfer between these two nonbonding orbitals does not change the bond strength, the effect of $\hat{l}_z$ is not shown. One

Table 1. Electron Occupation Numbers in TlH and Tl_2 of the Spin-Free Natural Orbitals Induced by the Spin−Orbit Coupling and the Electric Dipole Moments μ (Debye) in TlH

	TlH				Tl_2			
spin−orbit coupling	σ	σ^*	π^a	μ^b	σ_g	σ_u	π_u	π_g
neglected	1.9332	0.0661	0.0003 × 2	1.2958	1.8746	0.0432	0.0409 × 2	0.0002 × 2
included	1.9047	0.0678	0.0138 × 2	1.1821	1.8340	0.0447	0.0406 × 2	0.0202 × 2
Δ^c	−0.0285	0.0017	0.0135 × 2	−0.1137	−0.0406	0.0015	−0.0003 × 2	0.0200 × 2

[a] The multiplication by 2 for π orbitals reflects the degenerate occupation of the π_x and π_y components. [b] The dipoles are pointing from H to Tl. [c] The values with spin−orbit coupling included minus those where it is neglected.

dx.doi.org/10.1021/ct200457q |J. Chem. Theory Comput. 2011, 7, 2864–2875

should notice that both σ and σ^* orbitals have $m_{lz} = 0$ (where m_{lz} is the projection value of the orbital angular momentum along the z axis) and $\langle\sigma|\{\hat{l}_x, \hat{l}_y, \hat{l}_z\}|\sigma^*\rangle = 0$. Therefore, no electron can be directly transferred between the two orbitals by rotation, and any possible transfer has to be mediated by a transfer to a π orbital. This secondary electron promotion explains the negligible increase of the σ^* orbital occupation in the 0^+ wave function, so the weakened bond in TlH is due to the loss of the bonding, rather than a direct increase in the antibonding effect. The electric dipole moments for the $^1\Sigma^+$ and 0^+ wave functions are calculated and the reduction of the dipole by 0.1137 D is consistent with the fact that more electrons are located at the Tl center of the molecule by the electron transfer from the bonding to the nonbonding orbitals, and the positive charge of the region near Tl is reduced.

A similar investigation is also performed for Tl_2. For computational efficiency, we employed our newly developed ZFK3[77] model core potential and basis set for Tl, and the spin−orbit effect in this potential is at the level of DKH1.[78,79] The active space includes six orbitals with two electrons distributed among them. CASSCF geometry optimization for the first $^1\Sigma_g^+$ term gives the equilibrium internuclear distance of 3.507 Å. The $^1\Sigma_g^+$ term is of interest because it has the σ_g^2 electron configuration, which is similar to the σ^2 configuration of TlH that we just discussed, and the two cases can be compared. One should note that several studies[67,80−82] determined that the actual spin−orbit ground state of Tl_2 is the 0_u^- level stemming from the $^3\Pi_u$ term. Therefore, the $^1\Sigma_g^+$ term considered here is not the overall ground state but only the lowest $^1\Sigma_g^+$ term, used here for illustrative purposes.

At the equilibrium internuclear distance, CASCI is used to generate the $^1\Sigma_g^+$ wave function and the associated six one-component natural orbitals, σ_g, π_u, σ_u, and π_g, which are depicted in Figure 2a−d, and their occupation numbers are listed in Table 1. All of the *gerade* Γ-S terms generated with the active space of distributing two electrons in the six natural orbitals are used as the multielectron basis for the subsequent spin−orbit CI calculation to produce the spin−orbit 0_g^+ wave function. Only the gerade (g) terms are considered because the spin−orbit operator conserves parity, and we focus mainly on the spin−orbit influence on the $^1\Sigma_g^+$ term. The averaged occupation numbers of the one-component natural orbitals are obtained through the same procedure as the TlH case, and they are also listed in Table 1. As in the TlH case, the electron occupation in the bonding σ_g orbital is substantially depleted (0.0406), and most of this depletion is deposited into the antibonding π_g orbitals. Because of the even parity of the spin−orbit operator, only orbitals with the same parity can be coupled, which explains the correspondence between the electron depletion of the σ_g and the electron deposition on the π_g orbital. The electron transfer between the π_u and σ_u orbitals is insignificant, since they are barely occupied in the $^1\Sigma_g^+$ wave function. Employing the aforementioned effective bond order model, we calculate the bond order of Tl_2 to be 0.9564 for the $^1\Sigma_g^+$ and 0.9150 for the 0_g^+ wave function. Apparently, the decrease of the bond order for Tl_2 (0.0414) is greater than that for TlH (0.0152), consistent with the increase of the number of heavy atoms (Tl). However, considering the different basis sets used for the two molecules (without polarization functions for TlH, with polarization functions for Tl_2), this bond order change comparison is only qualitative.

Figure 2e,f demonstrates the electron transfer induced by the $\hat{l}_i\hat{s}_i$ components ($i = x, y$) of the spin−orbit operator. Similar arguments as for Figure 1d,e can be made, except that the inversion

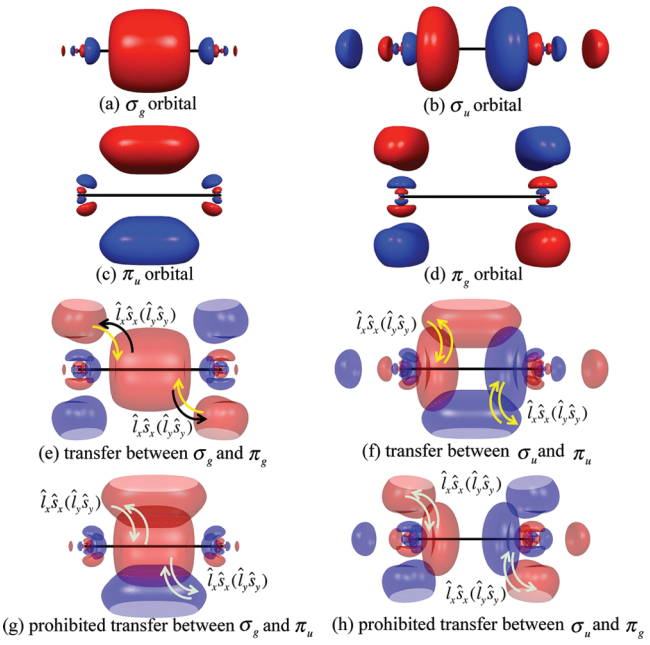

Figure 2. One-component natural CASCI orbitals (a−d) of Tl_2 and the spin−orbit coupling induced electron transfer (e−h) among them. In e−h, the $\hat{l}_x$ and $\hat{l}_y$ operators centered on the two Tl centers cause the electron transfer to (or from) the π_y and π_x orbitals, respectively. The substantial transfers are denoted by a black arrow, the negligible ones by yellow, and the prohibited ones by gray.

symmetry adds to the correlated electron rotation (transfer) around the two Tl nuclei, which is reflected in the inversion-symmetric pairwise arrangement of the curved arrows in Figure 2e,f. Actually, Figure 2e−h provides a graphical description of the even parity of the spin−orbit interaction. If the spin−orbit induced in-phase rotation (red to red or blue to blue) is energetically favorable, then the inversion-symmetrically correlated electron motion guarantees that this effect at the two Tl centers adds up in Figure 2e,f. This accumulation effect also applies if the out-of-phase (red to blue or blue to red) is energetically favorable instead. In contrast, in Figure 2g,h, an in-phase rotation on one side of the molecule must correspond to an out-of-phase rotation on the other side, and the spin−orbit effects cancel out. Therefore, any g−u electron transfer results in a null energy gain, and the spin−orbit effect must conserve the parity of the orbitals.

One might argue that the spin−orbit antibonding effect leads to a very substantial reduction of the dissociation energy (D_e), incommensurate with the reduction of bond order presented in this work. For example, in our recent study of TlH,[38] the reduction of the dissociation energy is about 0.4 eV at the CI level, 1/5 of the D_e of the $^1\Sigma^+$ state, while the reduction of bond order in the present work is just 1.6%. Furthermore, the 0_g^+ level of Tl_2 was predicted to be purely repulsive,[80] but our natural orbital analysis still predicts substantial bonding. This is because we focus only on the wave function change induced by the spin−orbit interaction without considering the explicit energy effects. At the dissociation limits for both TlH and Tl_2, the Tl 6p orbitals are all degenerate, and there is no energy cost for the spin−orbit induced electron transfer among them. Therefore, the spin−orbit stabilization leads to its maximum energy lowering at the dissociation limits. However, the degeneracy of the 6p orbitals is lifted as the covalent

bonds are formed, and the bonding electron pair tends to occupy the orbitals with lower energies (σ for TlH and σ_g for Tl_2). Consequently, the spin−orbit induced rotation will have to promote the electron from the low-energy orbitals to the high-energy orbitals, and this additional energy cost quenches the spin−orbit interaction and consequently reduces the amount of the spin−orbit energy lowering. This can also be understood as the covalent interaction hindering the spin−orbit induced electron transfer. The R-dependent spin−orbit stabilizations cause the large reduction of D_e for the 0^+ level of TlH and the purely repulsive potential energy curve for the 0_g^+ level of Tl_2. This effect cannot be revealed by considering only the wave functions at the equilibrium internuclear distances. In fact, there are many factors that together determine the bond energy, and it has been pointed out[73] that in general there is no direct correlation between bond order and bond energy.

Although only diatomic molecules are considered in this section, the concept presented here can be straightforwardly generalized to other molecules. For polyatomic molecules, there could be mixed bonding, antibonding, and nonbonding character in each one-component natural orbital, and this may complicate the analogous analysis. To solve this problem, one may use Weinhold's natural bond orbitals,[83−86] which have clear bonding, antibonding, or nonbonding character, as the basis to obtain the natural spinors. Before closing this section, we would like to once again emphasize that the computational methods and basis sets for TlH and Tl_2 were chosen to produce two bonding models that manifest interplay between covalent and spin−orbit interactions. One can use our analysis at higher levels such as the natural spinors from the energetically accurate multireference CI method.

4. HOW SPIN−ORBIT COUPLING QUENCHES THE JAHN−TELLER DISTORTION

In qualitative terms (see Figure 2.9 of ref 87), the Jahn−Teller distortion is caused by a nontotally symmetric electronic distribution in one of the degenerate electronic states. Under that circumstances, the symmetry of the Coulomb interactions between the nuclei and electrons is lowered, and the molecular structure is distorted correspondingly.[87,88] It has been reported that the spin−orbit interaction can quench the Jahn−Teller effect, and two simple but enlightening examples are Pb_3^+ [42] and WF_5.[41] Without considering the spin−orbit effect, the excited states of Pb_3^+ and the ground state of WF_5 suffer a strong Jahn−Teller distortion and change their structures from D_{3h} to C_{2v} symmetry. When the spin−orbit coupling is considered, however, those energetic minima are shifted back to the D_{3h} structure. This can be explained either by the fact that the spin−orbit interaction splits the electronic degeneracy and removes the driving force for the distortion or that the spin−orbit interaction introduces new symmetry operations of the double group, and the distortion based on point group arguments may not happen in the double group context.[43,89] To the best of our knowledge, the studies of this quenching effect have so far been based on the multielectron wave functions, with the focus placed on the spin−orbit and vibronic coupling between different electronic terms. Although this multielectron picture is natural for physicists, it does not serve as a good illustration in terms of the orbital picture of interactions. Therefore, an orbital-based explanation of this quenching would be informative, and in the present section we will use the natural spinors to illustrate

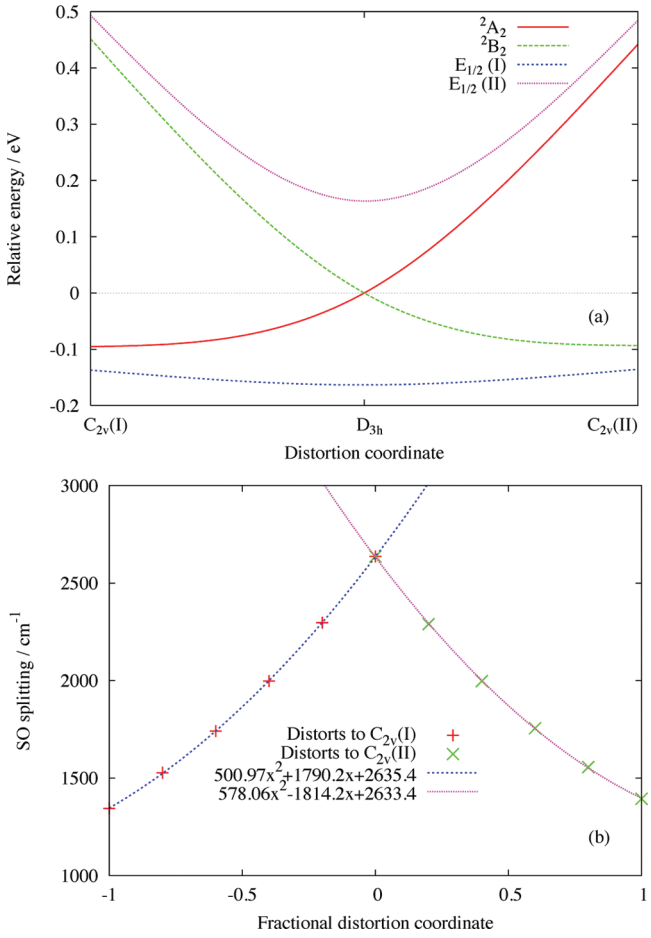

Figure 3. (a) Energetic profile of the Jahn−Teller distortion of WF_5. The term and level symbols are labeled as in the C_{2v} point group and double group. The curves are obtained by cubic-splines fitting to the energies calculated at the three labeled structures. (b) The spin−orbit splitting along the fractional distortion coordinate. From 0 to −1 is the $^2A_2$ distortion channel to the C_{2v}(I) structure and from 0 to 1 is the $^2B_2$ distortion channel to the C_{2v}(II) structure. The equations of the two fitted quadratic curves are also shown.

this quenching effect, with WF_5 as an example. In this work, we only focus on the traditional Jahn−Teller distortion that is induced by the electrostatic interaction. The recently formulated spin−orbit induced Jahn−Teller effect[48,49] is not considered here.

For computational efficiency, we employed the SBKJC effective core potentials (ECP) and basis sets.[90−92] Correspondingly, the spin−orbit adapted effective charges[93,94] were used for the spin−orbit CI calculations. We optimized the WF_5 structure both in D_{3h} and in the C_{2v} symmetry. In the D_{3h} optimization, the CASSCF calculation with one electron being distributed in the e'' degenerate orbitals is performed to calculate energy, while in the C_{2v} optimization the restricted open-shell Hartree−Fock (ROHF) is employed (which is equivalent to the CASSCF in D_{3h}, because there is only one occupied orbital instead of two). There are two distorted C_{2v} structures, whose ground states are $^2A_2$ and $^2B_2$, and we label them as C_{2v} (I) and C_{2v} (II), respectively. The $^2A_2$ and $^2B_2$ states cross at the D_{3h} symmetry and form the two components of the $^2E''$ state. The energetic profile of the distortion is illustrated in Figure 3a. The relative energies of these states and structural parameters of the three

Table 2. Bond Lengths (in Å), Angles (in Degrees) and Relative State Energies (eV) of the D_{3h} and the Two C_{2v} Structures of WF_5[a]

	W_1-F_3	W_1-F_6	W_1-F_5	$F_4-W_1-F_5$	$^2A_2$	$^2B_2$	$E_{1/2}$(I)	$E_{1/2}$(II)
D_{3h}	1.902	1.841	1.841	120.00	0.000	0.000	−0.163	0.163
C_{2v} (I)	1.904	1.826	1.846	109.80	−0.095	0.452	−0.137	0.493
C_{2v} (II)	1.904	1.854	1.831	129.53	0.442	−0.093	−0.136	0.484

[a] Term symbols are assigned according to the C_{2v} point group and its double group. The energy of the $^2E''$ state for the D_{3h} structure is taken to be the zero energy.

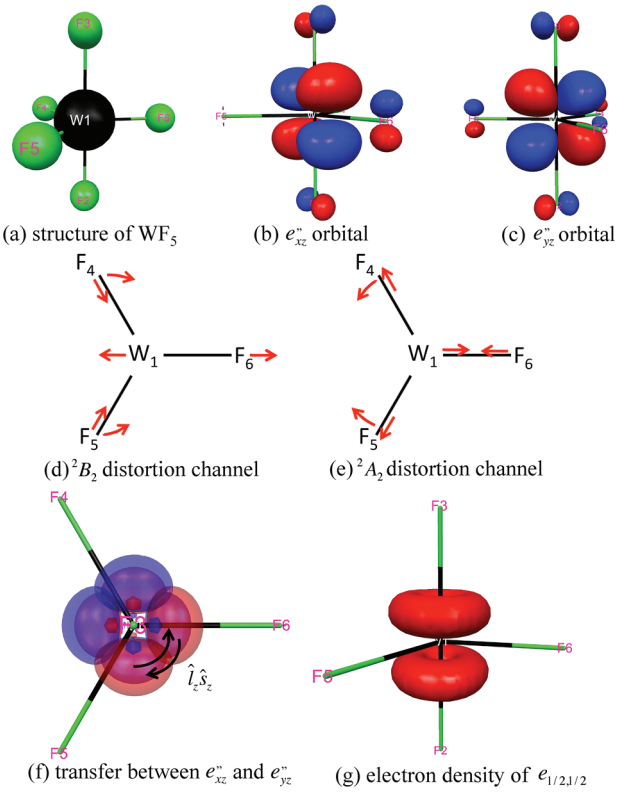

Figure 4. Structure (a), CASCI natural orbitals (b,c), distortions (d,e), spin−orbit induced electron transfer (f), and natural spinor electron density (g) of WF_5. The $\hat{l}_z$ operator in g is centered on W.

structures are listed in Table 2. The atoms are labeled according to Figure 4a. In this discussion, the $F_3-W_1-F_2$ and F_6-W_1 axes are the principal axes for the D_{3h} and C_{2v} structures, respectively.

Going from the C_{2v}(I) to D_{3h} and to C_{2v}(II) structures, the W_1-F_6 bond is lengthened. The W_1-F_4 and W_1-F_5 bonds are shrunk equivalently, and the $F_4-W_1-F_5$ angle opens up. This is the Jahn−Teller distortion coordinate. The structural parameters in Table 2 indicate that the $F_4-W_1-F_5$ angle changes more substantially than all of the W−F bond lengths in the distortion. Therefore, the distortion coordinate is mainly of a bending nature. The $^2A_2$ and $^2B_2$ terms ($^2E''$ term at the D_{3h} structure) are included in the spin−orbit coupling, and the energies of the resultant spin−orbit wave functions ($E_{1/2}$ and $E_{3/2}$ levels at the D_{3h} structure and $E_{1/2}$(I) and $E_{1/2}$(II) levels at the C_{2v} structures) are also listed in Table 2. The results from our calculations are qualitatively consistent with those of the previous DFT study of Dyall,[41] with the correct term symbols (see ref 95) and structural parameters slightly different by about 0.01 Å. The lack of interelectron correlation in the present study suggests that Dyall's B3LYP structural parameters and energies are more reliable. However, the energy profile in Figure 3a indicates that our simple model captures all of the essences of the distortion and its spin−orbit quenching.

All of the atomic labels in this discussion follow Figure 4a. The electronic configuration of WF_5 at the D_{3h} structure is predicted to be $(e'')^1$, and the e'' orbitals are shown in Figure 4b and c. Taking the $F_3-W_1-F_2$ and F_6-W_1 axes to be z and x axes, we call the two orbitals e''_{xz} and e''_{yz} orbitals, characterizing their main d components at the W center. Taking the F_6-W_1 axis as the C_{2v} principal axis, the e''_{xz} and e''_{yz} orbitals correspond to the b_2 and a_2 orbitals. Obviously, the e''_{xz} orbital has antibonding character for the W_1-F_6 bond, and increasing the population in the e''_{xz} orbital (forming the $^2B_2$ term) elongates the bond. As a consequence of this elongation, the reduced repulsion between F_6 and the remaining equatorial fluorine atoms (F_4 and F_5), with each of the equatorial fluorine atoms carrying Mulliken charge of −0.457 a.u., leads to shorter F_4-W_1 and F_5-W_1 bonds, and consequently, the stronger F_4-F_5 repulsion leads to the larger $F_4-W_1-F_5$ angle. This distortion is illustrated by Figure 4d. The e''_{yz} orbital has antibonding character for the F_4-W_1 and F_5-W_1 bonds, and putting an electron in this orbital (forming the $^2A_2$ term) elongates the two bonds. Meanwhile, the $F_4-W_1-F_5$ angle tends to be smaller to reduce the out-of-phase overlap between the p_z orbitals on F_4 and F_5 and the d_{yz} orbital on W. Smaller repulsion between the two equatorial atoms F_4 and F_5 and the remaining equatorial atom F_6 leads to a shorter F_6-W_1 bond. This distortion is illustrated in Figure 4e. Since both e'' orbitals have the same antibonding character along the $F_2-W_1-F_3$ axis, the F_2-W_1 and F_3-W_1 bond lengths are unchanged along the distortion. This orbital analysis based on antibonding characters and electrostatic repulsion fully explains the distortion coordinate mentioned in the previous paragraph. Obviously, this distortion coordinate is a component of the e' vibrational normal mode of the D_{3h} point group, and hence, this Jahn−Teller distortion is a typical $E'' \otimes e'$ problem.[87]

The spin−orbit CI calculation for the $^2E''$ term produces two levels, each having a pair of Kramers doublets. The natural spinors of the two lower states are calculated to be

$$e_{1/2,1/2} = \frac{1}{\sqrt{2}} e''_{xz}\beta + \frac{i}{\sqrt{2}} e''_{yz}\beta;$$
$$e_{1/2,-1/2} = \frac{1}{\sqrt{2}} e''_{xz}\alpha - \frac{i}{\sqrt{2}} e''_{yz}\alpha \quad (9)$$

and those of the two higher states are

$$e_{3/2,3/2} = \frac{1}{\sqrt{2}} e''_{xz}\alpha + \frac{i}{\sqrt{2}} e''_{yz}\alpha;$$
$$e_{3/2,-3/2} = \frac{1}{\sqrt{2}} e''_{xz}\beta - \frac{i}{\sqrt{2}} e''_{yz}\beta \quad (10)$$

dx.doi.org/10.1021/ct200457q |J. Chem. Theory Comput. 2011, 7, 2864–2875

Each of them is singly occupied in the corresponding levels. We can assign the symmetry label $e_{1/2,1/2}$ to the first spinor easily, as the $XZ\beta + iYZ\beta$ combination only exists in the $d_{3/2,1/2}$ and $d_{5/2,1/2}$ spinors (Table S.II of ref 28) and it has $j_z = 1/2$, and all functions with $j_z = 1/2$ must be of the $E_{1/2}$ irreducible representation of the D_{3h} double group.[96] The remaining orbitals follow the same argument. Here "XZ" and "YZ" represent any functions sharing the same symmetry properties as the d_{xz} and d_{yz} spherical harmonics, and similar notation is used below without further specification. Obviously, this labeling is consistent with the decomposition of the direct product between the orbital and spin representations in the D_{3h} double group:

$$E'' \otimes E_{1/2} = E_{1/2} \oplus E_{3/2} \tag{11}$$

This relationship demonstrates the usefulness of Table S.II of ref 28 for fast symmetry labeling of the natural spinors. However, this trick can be used only when there are basis functions on the principal axis, although one may put ghost functions on the principal axis to meet this requirement. Also, one has to check whether the m_{jz} values can be uniquely associated with the double group irreducible representations. Despite all of these constraints, the tentative symmetry labeling by using this trick serves as a good starting point for the more rigorous labeling by checking the double group character tables.

The like spins in each of the natural spinors suggest that only the $\hat{l}_z\hat{s}_z$ component of the spin−orbit operator is involved. This is consistent with the fact that $\langle XZ|\hat{l}_z|YZ\rangle$ is the only nonzero matrix element of $\langle XZ|\{\hat{l}_x, \hat{l}_y, \hat{l}_z\}|YZ\rangle$. Because of the much larger spin−orbit interaction around the W nucleus, the orbital angular momentum operators discussed here are centered on W. The spin−orbit induced electron transfer from the e_{xz}'' to e_{yz}'' orbitals and vice versa are illustrated in Figure 4f. Using the concept of spherical tensors,[55] one can easily associate the combinations of $e_{xz}'' + ie_{yz}''$ and $e_{xz}'' - ie_{zy}''$ to the eigenfunctions of $\hat{l}_z$ with eigenvalues of +1 and −1. Thus, the associated spin functions of eqs 9 and 10 indicate the two $e_{1/2}$ orbitals are of antiparallel coupling nature, while the two $e_{3/2}$'s are of parallel coupling, and this explains the spin−orbit stabilization of the $E_{1/2}$ and destabilization of the $E_{3/2}$ level. Contrary to the $\hat{l}_x\hat{s}_x$ and $\hat{l}_y\hat{s}_y$ induced electron transfer in the TlH and Tl_2 cases discussed above, the two orbitals involved in the $\hat{l}_z\hat{s}_z$ induced electron transfer in WF_5 are degenerate, and therefore the transfer is not hindered energetically. This free rotation leads to equivalent contributions from the two e'' orbitals in the $e_{1/2}$ and $e_{3/2}$ orbitals, in strong contrast to the unequal orbital contributions in eqs 4 and 5. Equations 6 and 7 have the same contributions from the π_x and π_y orbitals, as they are also degenerate and the $\hat{l}_z\hat{s}_z$ induced electron transfer is also without hindrance. When the symmetry is broken to C_{2v} and the two e'' orbitals are split to a_2 and b_2 with different energies, the rotation is hindered. The natural spinors for the $E_{1/2}(\mathrm{I})$ state at the $C_{2v}(\mathrm{I})$ structure are calculated to be

$$\begin{aligned} e_{1/2} &= 0.966440a_2\alpha + 0.256892b_2\beta \\ &\approx 0.966440e_{yz}''\alpha + 0.256892e_{xz}''\beta \end{aligned} \tag{12}$$

and its Kramers pair, with each of them singly occupied for the two $E_{1/2}$ components. The label $e_{1/2}$ is assigned since $E_{1/2}$ is the only Fermion irreducible representation of the C_{2v} double group and the approximate equality in eq 12 associates the orbital labels to those of D_{3h} symmetry. (The a_2 and b_2 orbitals at this structure cannot be identical to the e'' orbitals at the D_{3h} structure since orbitals are relaxed in the course of distortion.) The dominance of $a_2\alpha$ reflects the difficulty of the spin−orbit induced electron transfer, which is also seen in the small amount of spin−orbit energy lowering (0.042 eV) compared to that at the D_{3h} symmetry (0.163 eV).

The hindering of the spin−orbit induced electron transfer is also reflected by the smaller spin−orbit splitting at the distorted structures. Figure 3b illustrates the decrease of the spin−orbit splitting along the distortions to the two C_{2v} structures from the D_{3h} reference. In this figure, the spin−orbit splitting is estimated as

$$|E_{E_{1/2}(II)}(\underline{R}) - E_{E_{1/2}(I)}(\underline{R})| - |E_{2A_2}(\underline{R}) - E_{2B_2}(\underline{R})| \tag{13}$$

i.e., subtracting the splitting between the $^2A_2$ and $^2B_2$ terms from the splitting between the $E_{1/2}(\mathrm{I})$ and $E_{1/2}(\mathrm{II})$ levels at a given structure $\underline{R}$. The molecular structures between the D_{3h} reference and the two C_{2v} limits are obtained by fractional interpolation. For example, a structure between the D_{3h} and $C_{2v}(\mathrm{II})$ structures is given by

$$\underline{R}(f) = \underline{R}(D_{3h}) + f(\underline{R}(C_{2v}(\mathrm{II})) - \underline{R}(D_{3h})) \tag{14}$$

where $\underline{R}$ stands for coordinate vector of all six atoms and f is the fractional distortion coordinate ranging from 0 to 1. For the convenience of comparison between the two panels of Figure 3, we plot the spin−orbit splittings along the $^2A_2$ distortion (i.e., $C_{2v}(\mathrm{I})$) channel versus the negative values of the fractions. The two fitted curves in Figure 3b indicate a linear decrease of the spin−orbit splitting in the vicinity of the D_{3h} structure along each direction of the distortion. This can be understood by considering a Taylor expansion of the energy with respect to the distortion coordinate at the vicinity of the D_{3h} structure. The linear term is given by the energy gradient. Let us examine the symmetry properties of the gradient terms of matrix elements of the spin−orbit operator between two states. The symmetry of the spin−orbit operator derivative is of the E' irreducible representation, i.e., the symmetry of the distortion coordinate. The three possible direct products of the two states for the matrix elements are

$$A_1' \notin E_{1/2} \otimes E' \otimes E_{1/2} \tag{15}$$

$$A_1' \notin E_{3/2} \otimes E' \otimes E_{3/2} \tag{16}$$

$$A_1' \in E_{1/2} \otimes E' \otimes E_{3/2} \tag{17}$$

We can conclude that the coupling between the $E_{1/2}$ and $E_{3/2}$ states is allowed by symmetry (A'_1 is the totally symmetric irreducible representation of the D_{3h} double group), and it is this interaction that results in the nonzero gradient and thus linear terms in the Taylor series describing the dependence of the spin-orbit splitting as a function of the distortion coordinate.

As a side issue, it is worthwhile to discuss why the $\hat{l}_z\hat{s}_z$ operator in Figure 4f can couple different spins (mixing α and β in eq 12) when the structure is distorted. The reason is that in the calculation at the C_{2v} structure, the z axis has been reoriented along the F_6−W_1 bond and so is the quantization of the spin. Consequently, the $\hat{l}_z\hat{s}_z$ operator in Figure 4f becomes a $\hat{l}_y\hat{s}_y$ operator. The original e_{zy}'' and e_{xz}'' orbitals become of symmetry XY and YZ, and they are only coupled by $\hat{l}_y$ in the new coordinates. Thus, the flipping of spin is the result of choosing the new coordinate. To justify this reasoning, we carry out the calculation again, this time choosing the same coordinate

frame as the one for the D_{3h} structure, and produce the natural spinors to be

$$e_{1/2} = 0.966440a_2\alpha + i0.256892b_2\alpha \approx 0.966440e''_{yz}\alpha + i0.256892e''_{xz}\alpha \quad (18)$$

and its Kramers pair. Obviously, the electron transfer in this new coordinate is induced by the $l_z s_z$ component of the spin−orbit interaction, and the spin-flipping is removed. This side issue reminds us of the importance of choosing the right coordinate for a meaningful discussion. It is often troublesome to switch between coordinate systems when using several different point groups for the same system because of the convention most programs use to define the principal and secondary axis orientations, and tedious care should be exercised in discussing the symmetry labels and following their interrelation when the symmetry is changed.

As a result of the unhindered electron transfer at the D_{3h} symmetry and equivalent contributions from the two e'' orbitals, the spatial part of the electron densities of all of the natural spinors has the symmetry $(X^2 + Y^2)Z^2$, and this cylindrically symmetric electron density is plotted in Figure 4g. Obviously, the Coulomb potential stemming from this cylindrical distribution belongs to the totally symmetric irreducible representation (A_1') of the D_{3h} point group. Hence, there is no nontotally symmetric force exerted by the electrons to the nuclei around W that can distort the D_{3h} symmetric nuclear configuration so the Jahn−Teller distortion is quenched. One may argue that as the two e'' orbitals are degenerate, even without the spin−orbit effect, we may freely combine them as eq 9 and have a totally symmetric electron density, and the Jahn−Teller distortion could be avoided from the beginning. However, if this totally symmetric electron distribution is not stabilized by the spin−orbit interaction, it can be easily distorted by any perturbation induced by the nontotally symmetric molecular vibration, and the Jahn−Teller distortion would be turned on. Actually, if the spin−orbit stabilization of the totally symmetric electron distribution is not strong enough, despite the degeneracy removal, the energy gain from the vibronic coupling can still recouple the $e_{1/2}$ and $e_{3/2}$ orbitals to produce nontotally symmetric electron distribution, leading to the so-called pseudo-Jahn−Teller distortion. In such a case, the D_{3h} minimum on the blue curve of Figure 3a would become a maximum, a transition state connecting two stable C_{2v} structures. This distortion originates from the vibronic mixing of two (or more) nondegenerate electronic states under nuclear displacements. The ratio between the square of the vibronic coupling constant and the energetic gap between the electronic states determines whether the distortion is allowed.[87,88] In the context of this work, the energetic gap is proportional to the strength of the spin−orbit interaction, and the stronger the spin−orbit interaction, the less likely the vibronic distortion. The relative energies in Table 2 indicate that the spin−orbit stabilization (0.163 eV) is more substantial than the Jahn−Teller stabilization (0.093 and 0.095 eV) and that is why the D_{3h} structure is stable. Generally, the competition between the spin−orbit stabilization and the vibronic stabilization determines whether the high symmetry structure can stably exist.[43] The comparison between the strong and weak spin−orbit interactions in the stabilization of the high-symmetry nuclear configuration is illustrated by Figure 5.

The discussion of the simple WF_5 example can be generalized as follows. In the high symmetry structure with electronic degeneracy, the spin−orbit induced electron transfer among the degenerate orbitals is unhindered and the spin−orbit effect is

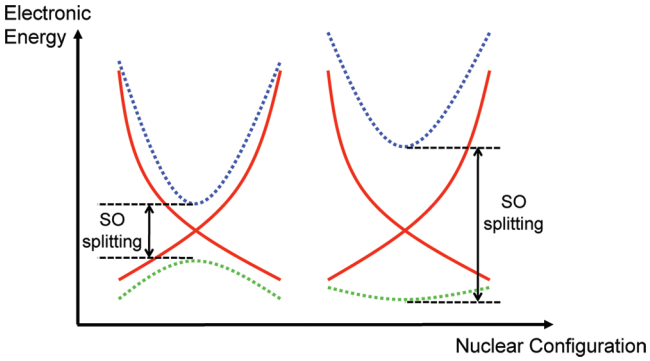

Figure 5. A schematic energy profile of the interplay between the spin−orbit (SO) interaction and the Jahn−Teller distortion. The red curves represent adiabatic potential energy curves without spin−orbit interaction, whereas the blue and green are with the interaction. On the left panel, the spin−orbit splitting is not strong enough to completely quench the Jahn−Teller distortion, resulting in the pseudo-Jahn−Teller distortion. On the right panel, the spin−orbit interaction is strong enough to stabilize the high-symmetry nuclear configuration. One should notice the similarity between Figure 3a and the right panel here.

maximized. Whenever this electron transfer produces a totally symmetric electron distribution that provides a totally symmetric Coulomb interaction with the nuclei, and the spin−orbit stabilization of this distribution is more significant than the possible energy lowering induced by the vibronic coupling, the Jahn−Teller distortion is quenched and the stable high-symmetry structure will exist. In other words, the spin−orbit interaction has an inherent symmetry-driven tendency to quench the electrostatic Jahn−Teller distortion, but it may not always have the strength to do so by sufficiently lowering the energy (clearly demonstrated in Figure 5, where the central high symmetry structure can have a higher or lower energy than the lower symmetry ones, depending on the magnitude of the splitting). Paradoxically, the electronic degeneracy that leads to the Jahn−Teller distortion also enlarges the spin−orbit interaction that quenches the distortion. One should note that although the spin−orbit interaction cannot split the degeneracy induced by the time-reversal symmetry (Kramers degeneracy), but neither can the vibronic coupling.[87,88] In this sense, for a system with an odd number of electrons, as long as the spin−orbit interaction splits all the electronic degeneracy into the double-valued Fermion irreducible representation of the corresponding double group and provides enough stabilization, the Jahn−Teller distortion is quenched. We would also like to emphasize that the spin−orbit effect may not completely split all of the electronic degeneracy to the Kramers 2-fold degeneracy, as for the T, O, and I type double groups, 4-fold Fermion irreducible representations are present.[89] For the molecules whose structures are of the corresponding point groups, the Jahn−Teller distortion can still occur with a spin−orbit coupled electronic wave function.

A common typical feature of covalent bonding and Jahn−Teller effects is their anisotropy (directionality): covalent bonds are directional as the kinetic pressure of the valence electrons of one bonding atom is attenuated in the direction of the other bonding atom;[61,64] the Jahn−Teller distortion proceeds along the specific direction (molecular vibrational mode) that favors a bonding interaction. It is for this reason that since the dawn of quantum chemistry, the Cartesian basis functions like p_x, p_y, and p_z are convenient, as they are the best

representations for such directional interactions, and the *rotational* analogues like p_{+1}, p_0, and p_{-1} are almost never used. Consequently, directional terminologies like "head-to-head" (for a σ bond) and "side-to-side" (for a π bond) have been used widely in chemistry education and research. In contrast, the spin−orbit interaction is intrinsically rotational, as the presence of angular momentum $\hat{\vec{l}}_{iA}$ in eq 1 shows, and its exertion is through a change of direction. The discussions in sections 3 and 4 reveal that the interplay between the spin−orbit and the bonding effect and Jahn−Teller distortion is caused by the competition between the rotational nature and the directional nature of the different interactions. This conclusion can be readily obtained from the orbital picture of the spin−orbit interaction, which is provided by the natural spinors.

To the best of our knowledge, this direction/rotation competition is proposed for the first time and can be extensively used to explain experimental or computational results in future studies of the spin−orbit effect in chemistry. For example, it can be used to quantitatively interpret the spin−orbit coupling in a metal pair of trinuclear copper complexes bridged by an oxygen ligand (Scheme 4 of ref 4) through the analysis of one-component orbital coefficients in the natural spinor expressions; also, it can be applied to quantitatively investigate the different Jahn−Teller distortion channels of the Tl_6^- cluster anion, which distorts from a cube to a parallelepiped when not considering spin−orbit interaction, but to a tetrahedral star otherwise.[98] There is one special advantage of using natural spinors in wave function analysis. Since the spinors are composed of the orbitals obtained in calculations without spin−orbit, they provide information about the changes induced by spin−orbit coupling to the wave function. In this sense, natural spinors are the natural language to explain any nontrivial spin−orbit effects in chemistry, and their potential utility should be more extensive than what was shown in the present paper.

5. CONCLUSION

In this work, we explored the utility of our newly developed natural spinors based on illustrative case studies. Two examples of TlH and Tl_2 molecules are presented to demonstrate how to use the natural spinors in order to rationalize the spin−orbit effect on bonding interactions (section 3). We demonstrated that the spin−orbit interaction will induce electron transfer among orbitals with different bonding, antibonding, and nonbonding characters (Figures 1 and 2 and Table 1) and affect the bond strength. A graphical description of the parity-conservation of the spin−orbit operator is also presented, connecting the conservation to the accumulation or cancellation of the spin−orbit effect. In section 4, we also used the natural spinors of the $E_{1/2}$ ground state of WF_5 to explain the spin−orbit quenching of the Jahn−Teller distortion (Figures 3 and 4 and Table 2). We demonstrated that the unhindered spin−orbit induced electron transfer among the degenerate orbitals can produce a totally symmetric electron distribution. If the spin−orbit stabilization of this distribution is large enough, the Jahn−Teller distortion is quenched (Figure 5). These illustrative cases demonstrate the power of natural spinors and the methods of analysis. The conclusions can be extended to general cases.

Davidson made the following comment about the natural orbitals in his comprehensive review of natural orbitals:[54] *the real advantage of natural orbitals is in getting maximum understanding for a fixed cost.* The results of the present work demonstrate that the understanding brought about by describing the spin-dependent relativistic effects with the aid of natural spinors can reach far beyond its original scope of electron correlation and lead us to a new vision of spin−orbit coupling. On the basis of the simple pictorial representations of natural spinors, we propose the hypothesis that any unexpected role that the spin−orbit interaction plays in chemistry is rooted in the competition between the rotational nature of the spin−orbit operator and the anisotropic interactions. This supposition provides the basis for the understanding of spin−orbit effects in chemistry.

AUTHOR INFORMATION

Corresponding Author

*E-mail: Mariusz.Klobukowski@ualberta.ca.

ACKNOWLEDGMENT

T.Z. expresses his gratitude to the Alberta Ingenuity Funds, Killam Trusts, and Alberta Scholarship Program for the student scholarships. M.K. thanks the Natural Sciences and Engineering Research Council of Canada for the support of the present project under Research Grant No. G121210414. M.W.S. acknowledges support by the DOE Chemical Physics program. The calculations were performed on the Linux clusters at the Department of Chemistry and Department of Academic Information and Communication Technologies at the University of Alberta. We are grateful to Professor M. S. Gordon for his continuing support of the development of the GAMESS-US program suite.

REFERENCES

(1) Desclaux, J. P.; Pyykkö, P. *Recherche* **1980**, *11*, 592–594.
(2) Pyykkö, P. *Chem. Rev.* **1988**, *88*, 563–594.
(3) Pyykkö, P.; Desclaux, J. P. *Acc. Chem. Res.* **1979**, *12*, 276–281.
(4) Pyykkö, P.; Desclaux, J. P. *C. R. Acad. Sci. Paris* **1981**, *292*, 1513–1515.
(5) Norrby, L. *J. Chem. Educ.* **1991**, *68*, 110–113.
(6) Pyykkö, P. *Angew. Chem., Int. Ed.* **2004**, *43*, 4412–4456.
(7) Pyykkö, P. *Inorg. Chim. Acta* **2005**, *358*, 4113–4130.
(8) Pyykkö, P. *Chem. Soc. Rev.* **2008**, *37*, 1967–1997.
(9) Schwerdtfeger, P.; Heath, G. A.; Dolg, M.; Bennet, M. A. *J. Am. Chem. Soc.* **1992**, *114*, 7518–7527.
(10) Visscher, L. *Chem. Phys. Lett.* **1996**, *253*, 20–26.
(11) Fedorov, D. G.; Gordon, M. S. Symmetry in Spin-Orbit Coupling. In *Low-lying Potential Energy Surfaces*; Hoffmann, M. R., Dyall, K. G., Eds.; American Chemical Society: Washington, DC, 2002; Vol. 828, pp 276−297.
(12) Marian, C. M. Spin-Orbit Coupling in Molecules. In *Reviews in Computational Chemistry*; Lipkowitz, K. B., Boyd, D. B., Eds.; WILEY-VCH: New York, 2001; Vol. 17, pp 99−204.
(13) Zeng, T. Ph.D. thesis, University of Alberta, Alberta, Canada, 2010
(14) Marian, C. M. Fine and hyperfine structure: Spin properties of molecules. In *Problem Solving in Computational Molecular Science: Molecules in Different Environments*; Wilson, S., Diercksen, H. F., Eds.; Kluwer Academic Publishers: Dordrecht, The Netherlands, 1997; pp 291−351.
(15) Fedorov, D. G.; Koseki, S.; Schmidt, M. W.; Gordon, M. S. *Int. Rev. Phys. Chem.* **2003**, *22*, 551–592.
(16) Fedorov, D. G.; Schmidt, M. W.; Koseki, S.; Gordon, M. S. Spin-orbit coupling methods and applications to chemistry. In *Recent Advances in Relativistic Molecular Theory*; Hirao, K., Ishikawa, Y., Eds.; World Scientific: Singapore, 2004; pp 107−136.

(17) Armbruster, M. K.; Weigend, F.; van Wüllen, C.; Klopper, W. *Phys. Chem. Chem. Phys.* **2008**, *10*, 1748–1756.
(18) Takahashi, O.; Saito, K.; Yabushita, S. *Int. J. Quantum Chem.* **1999**, *74*, 515–530.
(19) Bearpark, M. J.; Handy, N. C.; Palmieri, P.; Tarroni, R. *Mol. Phys.* **1993**, *80*, 479–502.
(20) Vallet, V.; Maron, L.; Teichteil, C.; Flament, J.-P. *J. Chem. Phys.* **2000**, *113*, 1391–1402.
(21) Das, K. K.; Petsalakis, I. D.; Liebermann, H.-P.; Alekseyev, A. B. *J. Chem. Phys.* **2002**, *116*, 608–616.
(22) Barandiarán, Z.; Seijo, L. *J. Chem. Phys.* **2003**, *118*, 7439–7456.
(23) Sánchez-Sanz, G.; Barandiarán, Z.; Seijo, L. *Chem. Phys. Lett.* **2010**, *498*, 226–228.
(24) Danilo, C.; Vallet, V.; Flament, J.-P.; Wahlgren, U. *J. Chem. Phys.* **2008**, *128*, 154310.
(25) Brozell, S. R.; Shepard, R. *J. Phys. Chem. A* **2009**, *113*, 12741.
(26) Stowasser, R.; Hoffmann, R. *J. Am. Chem. Soc.* **1999**, *121*, 3414–3420.
(27) Alekseyev, A. B.; Liebermann, H.-P.; Buenker, R. J. Spin-orbit multireference configuration interaction method and applications to systems containing heavy atoms. In *Recent Advances in Relativistic Molecular Theory*; Hirao, K., Ishikawa, Y., Eds.; World Scientific: Singapore, 2004; pp 65−105.
(28) Zeng, T.; Fedorov, D. G.; Schmidt, M. W.; Klobukowski, M. *J. Chem. Phys.* **2011**, *134*, 214108.
(29) Dagdigian, P. J.; Campbell, M. L. *Chem. Rev.* **1987**, *87*, 1–18.
(30) Bersuker, I. B.; Budnikov, S. S.; Leizerov, B. A. *Int. J. Quantum Chem.* **1977**, *11*, 543–559.
(31) Khudyakov, I. V.; Serebrennikov, Y. A.; Turro, N. J. *Chem. Rev.* **1993**, *93*, 537–570.
(32) Danovich, D.; Shaik, S. *J. Am. Chem. Soc.* **1997**, *119*, 1773–1786.
(33) van Koppeh, P. A. M.; Bowers, M. T.; Haynes, C. L.; Armentrout, P. B. *J. Am. Chem. Soc.* **1998**, *120*, 5704–5712.
(34) Roos, B. O.; Malmqvist, P. A.; Gagliardi, L. *J. Am. Chem. Soc.* **2006**, *128*, 17000–17006.
(35) Graves, C. R.; Yang, P.; Kozimore, S. A.; Vaughn, A. E.; Clark, D. L.; Conradson, S. D.; Schelter, E. J.; Scott, B. L.; Thompson, J. D.; Hay, P. J.; Morris, D. E.; Kiplinger, J. L. *J. Am. Chem. Soc.* **2008**, *130*, 5272–5285.
(36) Wang, X.; Andrews, L.; Malmqvist, P. A.; Roos, B. O.; Goncalves, A. P.; Pereira, C. C. L.; Marcalo, J.; Godart, C.; Villeroy, B. *J. Am. Chem. Soc.* **2010**, *132*, 8484–8488.
(37) Zeng, T.; Fedorov, D. G.; Klobukowski, M. *J. Chem. Phys.* **2009**, *131*, 124109.
(38) Zeng, T.; Fedorov, D. G.; Klobukowski, M. *J. Chem. Phys.* **2010**, *132*, 074102.
(39) Truflandier, L. A.; Brendler, E.; Wagler, J.; Autschbach, J. *Angew. Chem., Int. Ed.* **2011**, *50*, 255–259.
(40) Samet, C.; Rose, J. L.; Piepho, S. B.; Laurito, J.; Andrews, L.; Schatz, P. N. *J. Am. Chem. Soc.* **1994**, *116*, 11109–11119.
(41) Dyall, K. G. *J. Phys. Chem. A* **2000**, *104*, 4077–4083.
(42) Balasubramanian, K.; Majumdar, D. *J. Chem. Phys.* **2001**, *115*, 8795.
(43) Balasubramanian, K. *Mol. Phys.* **2010**, *107*, 797–807.
(44) Hisashima, T. A.; Matsushita, T.; Asada, T.; Koseki, S.; Toyota, A. *Theor. Chem. Acc.* **2008**, *120*, 85–94.
(45) Poluyanov, L. V.; Domcke, W. *J. Chem. Phys.* **2008**, *129*, 224102.
(46) Poluyanov, L. V.; Mishra, S.; Domcke, W. *Mol. Phys.* **2007**, *105*, 1471–1485.
(47) Poluyanov, L. V.; Mishra, S.; Domcke, W. *Chem. Phys.* **2007**, *332*, 243–248.
(48) Opalka, D.; Segado, M.; Poluyanov, L. V.; Domcke, W. *Phys. Rev. A* **2010**, *81*, 042501.
(49) Poluyanov, L. V.; Domcke, W. *Chem. Phys.* **2010**, *374*, 86–93.
(50) David, J.; Geurra, D.; Restrepo, A. *Inorg. Chem.* **2011**, *50*, 1480–1483.
(51) Pérez-Villa, A.; David, J.; Fuentealba, P.; Restrepo, A. *Chem. Phys. Lett.* **2011**, *507*, 57–62.
(52) Löwdin, P.-O. *Phys. Rev.* **1955**, *97*, 1474–1489.
(53) Löwdin, P.-O.; Shull, H. *Phys. Rev.* **1956**, *101*, 1730–1739.
(54) Davidson, E. R. Natural orbitals. In *Adv. Quantum Chem.*; Löwdin, P.-O., Ed.; Academic Press, Inc: New York, 1972; Vol. 6, pp 235−266.
(55) Zare, R. N. *Angular Momentum: Understanding Spatial Aspects in Chemistry and Physics*; John Wiley and Sons, Inc.: New York, 1988.
(56) Fedorov, D. G.; Gordon, M. S. *J. Chem. Phys.* **2000**, *112*, 5611–5623.
(57) Fedorov, D. G. Ph.D. thesis, Iowa State University, Ames, IA, 1999
(58) Schmidt, M. W.; Baldridge, K. K.; Boatz, J. A.; Elbert, S. T.; Gordon, M. S.; Jensen, J. H.; Koseki, S.; Matsunaga, N.; Nguyen, K. A.; Su, S.; Windus, T. L.; Dupuis, M.; Montgomery, J. A., Jr. *J. Comput. Chem.* **1993**, *14*, 1347–1363.
(59) Gordon, M. S.; Schmidt, M. W. Advances in electronic structure theory: GAMESS a decade later. In *Theory and Applications of Computational Chemistry: The First Forty Years*; Dykstra, C. E., Frenking, G., Kim, K. S., Scuseria, G. E., Eds.; Elsevier: Amsterdam, The Netherlands, 2005; pp 1167−1189.
(60) Bode, B. M.; Gordon, M. S. *J. Mol. Graphics Model.* **1998**, *16*, 133–138.
(61) Ruedenberg, K.; Schmidt, M. W. *J. Comput. Chem.* **2007**, *28*, 391–310.
(62) Bitter, T.; Ruedenberg, K.; Schwarz, W. H. E. *J. Comput. Chem.* **2007**, *28*, 411–422.
(63) Grundström, B.; Valberg, P. *Z. Phys.* **1938**, *108*, 326–337.
(64) Ruedenberg, K.; Schmidt, M. W. *J. Phys. Chem. A* **2009**, *113*, 1954–1968.
(65) Bitter, T.; Wang, S. G.; Ruedenberg, K.; Schwarz, W. H. E. *Theor. Chem. Acc.* **2010**, *127*, 237–257.
(66) Dyall, K. G.; Fægri, K., Jr. *Introduction to Relativistic Quantum Chemistry*; Oxford University Press: Oxford, U.K., 2007.
(67) Lee, Y. S. Two-component relativistic effective core potential calculations for molecules. In *Relativistic electronic structure theory: Part 2. Applications*; Schwerdtfeger, P., Ed.; Elsevier: Amsterdam, The Netherlands, 2004; pp 352−416.
(68) Klobukowski, M. *Chem. Phys. Lett.* **1993**, *214*, 166–174.
(69) Nakajima, T.; Hirao, K. *Chem. Phys. Lett.* **2000**, *329*, 511–516.
(70) Nakajima, T.; Hirao, K. *J. Chem. Phys.* **2000**, *113*, 7786–7789.
(71) Dunning, T. H. *J. Chem. Phys.* **1989**, *90*, 1007–1023.
(72) Huzinaga, S.; Andzelm, J.; Klobukowski, M.; Radzio-Andzelm, E.; Sakai, Y.; Tatewaki, H. *Gaussian basis sets for molecular calculations*; Huzinaga, S., Ed.; Elsevier: Amsterdam, The Netherlands, 1984.
(73) Roos, B. O.; Borin, A. C.; Gagliardi, L. *Angew. Chem., Int. Ed.* **2007**, *46*, 1469–1472.
(74) Kramers, H. A. *Proc. Acad. Sci. Amsterdam* **1936**, *33*, 959.
(75) Bethe, H. A.; Salpeter, E. E. *Quantum Mechanics of One- and Two-Electron Atoms*; Dover Publications, Inc.: Mineola, NY, 2008.
(76) Frenking, G.; Tonner, R. *Nature* **2007**, *446*, 276–277.
(77) Zeng, T.; Fedorov, D. G.; Klobukowski, M. *J. Chem. Phys.* **2010**, *133*, 114107.
(78) Hess, B. A. *Phys. Rev. A* **1986**, *33*, 3742.
(79) Jansen, G.; Hess, B. A. *Phys. Rev. A* **1989**, *39*, 6016.
(80) Pitzer, K. S. *Int. J. Quantum Chem.* **1984**, *25*, 131–148.
(81) Ermler, W. C.; Lee, Y. S.; Christiansen, P. A.; Pitzer, K. S. *Chem. Phys. Lett.* **1981**, *81*, 70–74.
(82) Ermler, W. C.; Ross, R. B.; Christiansen, P. A. Spin-orbit coupling and other relativistic effects in atoms and molecules. In *Advances in Quantum Chemistry*; Löwdin, P.-O., Ed.; Academic Press, Inc.: San Diego, CA, 1988; Vol. 19, pp 139−182.
(83) Foster, J. P.; Weinhold, F. *J. Am. Chem. Soc.* **1980**, *102*, 7211–7218.
(84) Read, A. E.; Curtiss, L. A.; Weinhold, F. *Chem. Rev.* **1988**, *88*, 899–926.
(85) Weinhold, F. Natural bond orbital methods. In *Encyclopedia of Computational Chemistry*; Schleyer, P. v. R., Ed.; John Wiley and Sons, Ltd.: Athens, GA, 1998; Vol. 3, pp 1792−1811.
(86) Weinhold, F.; Landis, C. R. *Chem. Educ. Res. Pract. Eur.* **2001**, *2*, 91–104.

(87) Bersuker, I. B. *The Jahn-Teller Effect*; Cambridge University Press: Cambridge, U.K., 2006.
(88) Bersuker, I. B. *The Jahn-Teller Effect and Beyond*; The Academy of Sciences of Moldova: Chişinău, Moldova; The University of Texas at Austin: Austin, TX, 2008.
(89) Balasubramanian, K. *Relativistic Effects in Chemistry Part A*; John Wiley and Sons, Inc.: New York, 1997.
(90) Stevens, W. J.; Basch, H.; Krauss, M. *J. Chem. Phys.* **1984**, *81*, 6026–6033.
(91) Stevens, W. J.; Krauss, M.; Basch, H.; Jasien, P. G. *Can. J. Chem.* **1992**, *70*, 612–630.
(92) Cundari, T. R.; Stevens, W. J. *J. Chem. Phys.* **1993**, *98*, 5555–5565.
(93) Koseki, S.; Gordon, M. S.; Schmidt, M. W.; Matsunaga, N. *J. Chem. Phys.* **1995**, *99*, 12764–12772.
(94) Koseki, S.; Schmidt, M. W.; Gordon, M. S. *J. Phys. Chem. A* **1998**, *102*, 10430–10435.
(95) We repeated the same DFT calculation in ref 41 and found that the $^2A_2$ and $^2B_2$ label assignments in Figure 1 of the reference should be swapped.
(96) Jacobs, P. *Group Theory with Applications in Chemical Physics*; Cambridge University Press: Cambridge, U.K., 2005.
(97) Yoon, J.; Mirica, L. M.; Daniel, T.; Stack, P.; Solomon, E. I. *J. Am. Chem. Soc.* **2004**, *126*, 12586–12595.
(98) Wedig, U.; Saltykov, V.; Nuss, J.; Jansen, M. *J. Am. Chem. Soc.* **2010**, *132*, 12458–12463.